Electrochemical Kinetics of Nanostructured Nb2O5 Electrodes

Jérémy Come, Veronica Augustyn, Jong Woung Kim, Patrick Rozier, Pierre-Louis Taberna, Pavel Gogotsi, Jeffrey W. Long, Bruce Dunn, Patrice Simon

Electrochemical Kinetics of Nanostructured Nb_2O_5 Electrodes

Jérémy Come,[a,b] Veronica Augustyn,[c] Jong Woung Kim,[c] Patrick Rozier,[a,b] Pierre-Louis Taberna,[a,b] Pavel Gogotsi,[d,e] Jeffrey W. Long,[d,*] Bruce Dunn,[c,*] and Patrice Simon[a,b,*,z]

[a]*Université Paul Sabatier, CIRIMAT UMR CNRS 5085, 31062 Toulouse Cedex 4, France*
[b]*Réseau sur le Stockage Electrochimique de l'Energie (RS2E), FR CNRS 3459, France*
[c]*Department of Materials Science & Engineering, University of California, Los Angeles, California 90095, USA*
[d]*Surface Chemistry Branch, Naval Research Laboratory, Washington, DC 20375, USA*

Pseudocapacitive charge storage is based on faradaic charge-transfer reactions occurring at the surface or near-surface of redox-active materials. This property is of great interest for electrochemical capacitors because of the substantially higher capacitance obtainable as compared to traditional double-layer electrode processes. While high levels of pseudocapacitance have been obtained with nanoscale materials, the development of practical electrode structures that exhibit pseudocapacitive properties has been challenging. The present paper shows that electrodes of Nb_2O_5 successfully retain the pseudocapacitive properties of the corresponding nanoscale materials. For charging times as fast as one minute, there is no indication of semi-infinite diffusion limitations and specific capacitances of 380 F g^{-1} and 0.46 F cm^{-2} are obtained in 40-μm thick electrodes at a mean discharge potential of 1.5 V vs Li^+/Li. In-situ X-ray diffraction shows that the high specific capacitance and power capabilities of Nb_2O_5 electrodes can be attributed to fast Li^+ intercalation within specific planes in the orthorhombic structure. This intercalation pseudocapacitance charge-storage mechanism is characterized as being an intrinsic property of Nb_2O_5 that facilitates the design of electrodes for capacitive storage devices. We demonstrate the efficacy of these electrodes in a hybrid electrochemical cell whose energy density and power density surpass that of commercial carbon-based devices.

The widespread interest in electrochemical energy storage reflects its impact on everyday applications, including portable electronics, hybrid vehicles and, to a lesser degree, the electric grid. Although batteries are far more pervasive, the use of electrochemical capacitors (ECs) as electrical energy storage devices is finding a number of applications where batteries are less suitable. One such example is regenerative braking, which requires fast and reversible charge storage as well as long-term cyclability.[1] The current technology of ECs is based upon charge storage at the electric double layer that is formed when a potential is applied at the interface between a high-surface-area material, typically carbon, and a liquid electrolyte. The charge storage is non-faradaic and specific capacitance generally scales with the specific surface area of the electrode material available for ion adsorption, leading to values of ∼150 F g^{-1} for activated carbon when the ion size matches the average pore size.[2] Non-faradaic surface adsorption gives rise to the typical response of a capacitor: currents that are inversely proportional to charging time and independent of potential, and charge-storage capacity that is mostly independent of rate. Such electrochemical double-layer capacitors (EDLCs) exhibit lower energy densities than those of lithium-ion batteries, where charge storage occurs in the bulk of the electrode material.[3]

Reversible faradaic reactions can also lead to capacitor-like behavior, a phenomenon that is called pseudocapacitance.[4] These charge-transfer reactions generally occur from ion adsorption or ion insertion at the surface or near-surface of the active material and lead to high levels of charge storage. The interest for such materials is the prospect of achieving high specific capacitance values (>1000 F g^{-1}) associated with the fast redox reactions while preserving the good power capability and cycle life that is typical of EDLCs. Designing high-performance pseudocapacitive materials is therefore a promising direction for increasing the energy density of ECs.

Transition metal oxides are the most well-studied pseudocapacitive compounds due to their high oxidation states and ease of synthesis.[5] One of the best examples of such materials is MnO_2, where it is suggested that protons or cations from the aqueous electrolyte migrate to the near-surface of the MnO_2 particles where they undergo a fast redox reaction resulting in a continuous change in the Mn oxidation state, from +4 to +3, within 0.9 V.[6] Like many other transition metal oxides, however, MnO_2 has low electronic conductivity (∼10^{-6} S cm^{-1}) so that specific capacitance values in excess of 1000 F g^{-1} are obtained only when active films are less than 2 μm.[7] High values of specific capacitance have also been reached with other transition metal oxides such as V_2O_5[8] and MoO_3.[9] These results underscore the point that careful attention must be paid when considering the high specific capacitance values reported for thin films. These values may be attributed to complete or nearly complete utilization of the redox-active oxide because of electron and ion accessibility to the thin layer of material.[10,11] While these fundamental studies are useful for identifying the maximum achievable capacitance and power capability of a material, the low mass loading results in high gravimetric or volumetric capacitance values at the expense of low areal capacitance (F cm^{-2}) values, making such electrodes impractical for medium and large-scale devices.

The present paper concerns the electrochemical properties of Nb_2O_5 and its utilization in high performance hybrid devices. Initial studies of this metal oxide showed that Li^+ intercalation occurs at a potential below 2 V vs. Li^+/Li,[12] and it was used as a cathode in a 2-V secondary battery with a Li metal anode.[13] The lithiation of $Li_xNb_2O_5$ proceeds up to $x = 2$, corresponding to a maximum theoretical capacity of 200 mAh g^{-1}. Various polymorphs of the material have been studied,[14] among which the pseudohexagonal (*TT*-Nb_2O_5) and orthorhombic phases (*T*-Nb_2O_5) are of interest to us because of the continuous change of potential with state of charge, indicating that the electrochemical reaction is occurring within a single phase material.

More recent studies on the electrochemical properties of Nb_2O_5 films showed that crystalline forms of these materials were capable of exhibiting high capacitance and high rate capability.[15] Using kinetic analyses, we determined that the pseudocapacitive response of *T*-Nb_2O_5 is not due to surface redox reactions but rather to fast two-dimensional Li^+ transport within the crystal structure that causes no phase changes during the electrochemical reaction,[16] a behavior that is termed intercalation pseudocapacitance. That is, charge storage occurs due to fast Li^+ intercalation while the current is linearly proportional to the sweep rate. Pseudocapacitive behavior is preserved even in thick films of 40 μm, indicating that Nb_2O_5 offers faster Li^+ intercalation than $Li_4Ti_5O_{12}$,[17] with specific capacity on the order of 120 mAh g^{-1} at a 60 *C*-rate (1.2 Li^+ per Nb_2O_5 exchanged in 1 minute).

In this paper we take the important next step of demonstrating that the intercalation pseudocapacitance charge-storage mechanism can

*Electrochemical Society Active Member.
[e]Present address: Drexel University, Philadelphia, Pennsylvania 19104, USA.
[z]E-mail: simon@chimie.ups-tlse.fr

be extended to practical electrode structures. In particular, we address the question of whether the kinetics for 40 μm-thick electrodes are comparable to the behavior of the thin films reported previously, and if a bulk process continues to dominate the charge-storage properties. In addition, kinetic studies and in-situ X-ray diffraction measurements show that intercalation pseudocapacitance in Nb_2O_5 is an intrinsic property of the material which, in turn, suggests a route for achieving high capacitance values in practical electrode structures. Finally, we demonstrate a high-power hybrid electrochemical energy storage device using *T*-Nb_2O_5 as the negative electrode and activated carbon as the positive electrode.

Experimental

Synthesis.— The synthesis and structural characterization of *T*-Nb_2O_5 particles were reported in an earlier paper.[15] Briefly, the *T*-Nb_2O_5 was obtained by using an aqueous sol–gel route. First, anhydrous $NbCl_5$ was dissolved in ethanol, while a solution of deionized water and ethanol was prepared in a separate vial. After cooling for 2 h, both solutions were mixed together. Propylene oxide was then gradually injected until a transparent gel formed. After aging for 24 h, the gel was placed in acetone for 5 days and supercritically dried in CO_2. Finally, the resulting aerogel was annealed at 600°C for 2 h to obtain 35-nm nanocrystals with the orthorhombic structure.

In-situ XRD.— In-situ X-ray diffraction (XRD) measurements were performed using an electrochemical cell described previously.[18] The positive electrode in this cell, Nb_2O_5 powder mixed with carbon black (weight ratio 80:20) with no binder, was placed behind an X-ray transparent beryllium window which also acted as a current collector for the Nb_2O_5 electrode, while Li metal served as the negative electrode. The two electrodes were separated by a glass fiber separator (Whatman, GF/A) saturated with 1M $LiClO_4$ in propylene carbonate (PC). X-ray diffraction patterns were taken on a Bruker D8-Advance diffractometer using monochromatic Cu Kα radiation ($\lambda = 1.5418$ Å) and a Lynx-Eye detector. X-ray patterns were measured in the 15–60° 2θ range in a step-scan mode with a counting time of 1 s and an angular step width of 0.02° 2θ. The cell was discharged and charged at a rate of *C*/5. X-ray diffraction patterns for $Li_xNb_2O_5$ were collected every $x = 0.2$ during a relaxation period of 1 hour. The *c*-axis lattice parameter refinement was performed using FullProf Software.

Electrode preparation.— Thick Nb_2O_5 electrodes were prepared by mixing the active material, carbon black (Timcal Super C65) and polyvinylidene fluoride (PVdF) binder in a 80:10:10 weight ratio in *N*-methyl-2-pyrrolidinone (NMP). The slurry was drop cast onto 12-mm diameter aluminum disk current collectors and dried at 80°C for 12 hours.

To prepare activated carbon electrodes, 95 wt% of commercially available microporous carbon powder (YP17, Kuraray Chemical Co., LTD, Japan) was mixed with 5 wt% of polytetrafluoroethylene binder (PTFE, 60 wt% in H_2O, Sigma) in ethanol until a thick slurry was formed. The paste was cold-rolled and 12-mm disks were punched. The mass loading was then adjusted depending on the Nb_2O_5 active mass material. The freestanding electrode was placed onto a carbon-treated aluminum current collector to decrease the contact resistance.[19] Finally, the electrodes were dried at 120°C in vacuum for 12 h.

Electrochemical characterization.— The electrochemical properties of the Nb_2O_5 electrodes were characterized using 3-electrode Swagelok cells with a potential range between 1.2 V and 3 V (vs. Li/Li^+). The Nb_2O_5 electrode served as the working electrode, activated carbon as the counter electrode, 1M $LiClO_4$ in PC saturated into a glass fiber separator (Whatman, GF/A) as the electrolyte, and lithium foil was used as the reference electrode. In these measurements, the conventional Li metal counter electrode was replaced with an over-capacitive activated carbon electrode in order to limit polarization resistance.

For testing the Nb_2O_5/carbon hybrid cell, a Nb_2O_5 composite negative electrode was coupled with an activated carbon positive electrode. The Nb_2O_5 mass loading of the negative electrode was set to 1.5 mg cm^{-2}. The activated carbon/Nb_2O_5 mass loading ratio was calculated according to the gravimetric capacities of both materials at 100 mA g^{-1}, *i.e.* 140 mAh g^{-1} and 30 mAh g^{-1}, respectively. Hence, the positive/negative active material mass ratio was set to 4.7, leading to an activated carbon mass loading of ca. 7 mg cm^{-2}.

Rate performance of the hybrid cell was compared to that of a carbon/carbon EDLC tested in LP30. The LP30 electrolyte consists of 1M $LiPF_6$ salt dissolved in a mixture of ethylene carbonate (EC) and dimethylcarbonate (DMC) in a 1:1 volume ratio. Typically, 7 mg cm^{-2} films were used for the power tests. Ragone plot data are extracted from galvanostatic cycling at different current densities.

Cells were assembled in an argon-filled glove box with oxygen and moisture levels of < 1 ppm. All electrochemical measurements were carried out using a Bio-Logic VMP3 potentiostat. The gravimetrically-normalized capacitance values reported in this paper were based on the weight of the active material, Nb_2O_5.

Results

In-situ XRD measurements.— In-situ XRD, coupled with electroanalytical characterization, was used to determine whether Li^+ intercalation occurred within the bulk material or only within the surface or subsurface regions. Kumagai et al. reported an in-situ XRD investigation on micrometer-sized *T*-Nb_2O_5 particles and showed that Li^+ was inserted in a single-phase reaction, with minimal change in unit cell volume.[20] Moreover, it appeared that Li^+ was preferentially inserted in the (180) and (001) planes, a feature that was confirmed in a recent ex-situ TEM study.[15] Figure 1a shows XRD patterns collected during various lithiation and delithiation states during the cycling of the

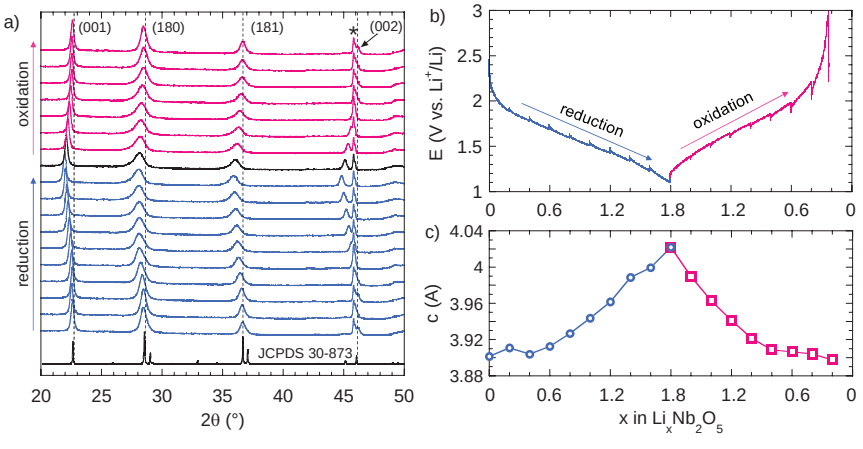

Figure 1. a) XRD patterns collected for $Li_xNb_2O_5$ during electrochemical cycling every $x = 0.2$. The star (*) denotes the (001) diffraction peak of the Beryllium window that was used as current collector; b) Corresponding charge/discharge curves showing relaxation periods during which the XRD patterns were collected; c) *c*-axis lattice parameter evolution as a function of *x* in $Li_xNb_2O_5$.

Nb_2O_5 electrode (shown in Fig. 1b). The diffraction patterns are consistent with the orthorhombic structure of *T*-Nb_2O_5 (JCPDS 30–873). Among the observed Bragg peaks, only the (00*l*) reflections are unique and allow for accurate determination of the *c*-axis lattice parameter. The diffraction peaks indexed as (180) and (181) are comprised of several different (*hkl*) contributions and thus prevent an accurate determination of *a* and *b* lattice parameters.[21] Nonetheless, the *c*-axis lattice parameter provides important insight regarding the structural changes that occur upon cycling. The fact that diffraction peaks neither appear nor disappear during electrochemical cycling confirms that the redox reaction of Li^+ with Nb_2O_5 occurs in a one-phase system. On lithium intercalation, the diffraction peaks shift toward lower diffraction angles, indicating an increase in the interplanar distances. This increase is consistent with the presence of larger Nb^{4+} cations (ionic radius: 0.83 Å) as compared to the smaller Nb^{5+} cations (ionic radius: 0.78 Å) in combination with Li^+ intercalation in the empty sites of the *T*-Nb_2O_5 structure. Upon lithium removal, the diffraction peaks shift toward higher diffraction angles, indicating lattice contraction. Figure 1c shows the evolution of the *c*-axis lattice parameter as a function of the state of charge. For the initial state, the lattice parameter is estimated to be 3.91 Å, close to the theoretical value of 3.93 Å.[21] After lithium intercalation to $x = 1.8$ (based on $Li_xNb_2O_5$), the *c*-axis lattice parameter increased to 4.02 Å. Upon lithium removal, the lattice parameter decreased to its initial value. These results suggest that the {001} family of planes form energetically favorable pathways for facile Li^+ transport in the structure, a feature indicated in the work of Kumagai et al.[20] and recent DFT calculations.[22] Moreover, these measurements show that reversible Li^+ intercalation/extraction is a bulk process in the *T*-Nb_2O_5 electrode and not confined to a thin layer at the outer surface, and occurs with small crystallographic change in Nb_2O_5.

Electrochemical kinetics characterization.— A cross-section of a typical Nb_2O_5 electrode is shown in Figure 2a. Film thickness is approximately 40 ± 5 μm, with a mass loading between 1 and 1.5 mg cm^{-2}. Cyclic voltammograms for sweep rates from 5 to 100 mV s^{-1} (Figure 2b) are comparable to those reported earlier for nanocrystalline Nb_2O_5 films of low mass loading (20 μg cm^{-2}).[15] These measurement conditions correspond to a charge or discharge time between 240 and 12 seconds. Cyclic voltammetry for a Nb_2O_5 electrode taken at a sweep rate of 20 mV s^{-1} over the potential range between 2 V and 1.2 V vs. Li^+/Li is shown in Figure 3a. The nearly rectangular shape of the voltammogram is very similar to that of hydrous RuO_2 in H_2SO_4,[4] and is characteristic of the continuous change in oxidation state of a pseudocapacitive material during the charge–discharge process. It is commonly accepted that in a sweep voltammetry experiment, the current is characterized by a power law:

$$I = av^b \quad [1]$$

where *I* is the current (A), *v* is the potential sweep rate (V s^{-1}), *a* and *b* are arbitrary coefficients.[23] From the current response, it is possible to separate the capacitive contribution (*I* proportional to *v*) from the purely diffusion-limited contribution (*I* proportional to $v^{1/2}$). In Figure 3b, the anodic and cathodic peak currents determined from the voltammograms of Fig. 2b are plotted as a function of sweep rate between 1 and 100 mV s^{-1}. The *b*-coefficient of Eq. 1 is equal to 1 and 0.95 for cathodic and anodic currents, respectively. Thus, it is evident that the total stored energy in the Nb_2O_5 arises from an electrochemical process that is not limited by solid state diffusion (Li^+ diffusion in Nb_2O_5), similar to what was observed with thin films of Nb_2O_5 particles.[16] In contrast, battery electrode materials are generally characterized by $b = 0.5$, indicative of a semi-infinite diffusion process.[24,25] Thus, the linear response exhibited here underscores the fundamental difference between Nb_2O_5 and conventional Li^+ intercalation battery materials, and highlights the outstanding rate performance of the Nb_2O_5.

The sweep-rate dependence of the specific capacitance indicates that the Nb_2O_5 electrode retains some 90% of its maximum capacitance, 380 F g^{-1}, for charge–discharge times on the order of 1 minute (Figure 3c). The gravimetric capacitance values for the Nb_2O_5 composite electrode are only ~10% less than that of the thin nanocrystalline film (20 μg cm^{-2} loading), despite the fact that its Nb_2O_5 mass loading is over 50 times higher.[15] This amount of capacitive storage represents further evidence that the high rate performance of Nb_2O_5 does not depend on the electrode loading at least for thicknesses up to 40 μm.

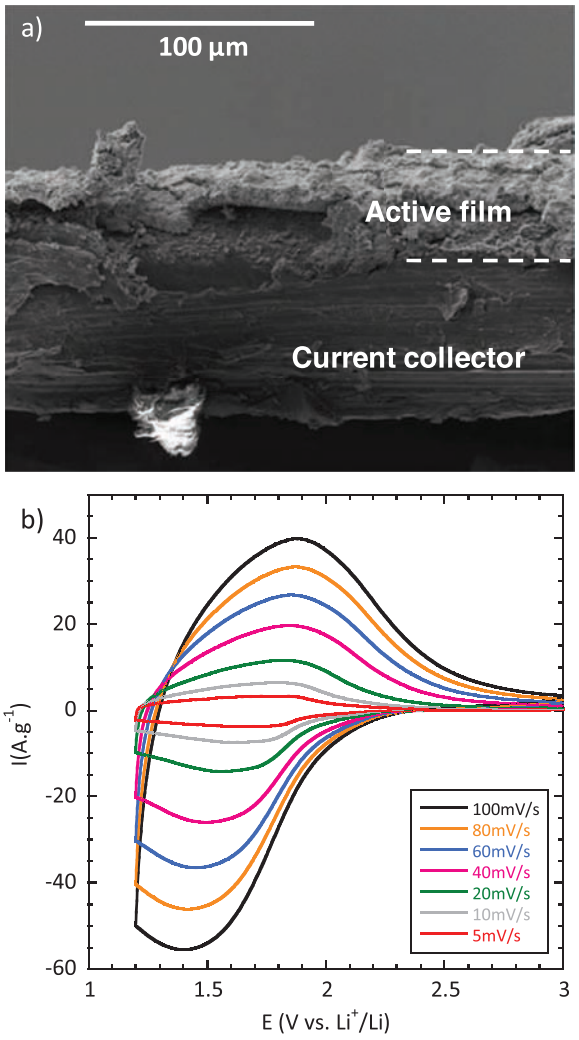

Figure 2. a) Cross-sectional view of Nb_2O_5 composite film deposited onto the aluminum current collector, and b) cyclic voltammetry curves of the Nb_2O_5 electrode from 5 mV s^{-1} to 100 mV s^{-1}.

Another important metric for capacitive charge storage is the area-normalized capacitance (F cm^{-2}), as this value provides an indication of performance in a practical electrode structure and corresponding device. The areal capacitance determined for 1.2 mg cm^{-2} Nb_2O_5 electrodes is only slightly sweep-rate dependent. Values in the range of 0.5 F cm^{-2} are obtained for charge/discharge times of 1 minute and longer (Figure 3c). By comparison, activated carbon electrodes for conventional EDLCs exhibit values in the range of 0.4 to 2 F cm^{-2}.[26–31] It is interesting to note that even though transition metal oxides such as MnO_2 or V_2O_5 exhibit high specific capacitance, on the order of 1000 F g^{-1}, the areal capacitance values are typically in the range of 1 mF cm^{-2} because of the very thin nature of the oxide film.[32,33] Thus, the high specific capacitance achieved in thin films of one micron (or less) have yet to be translated into viable electrode structures.

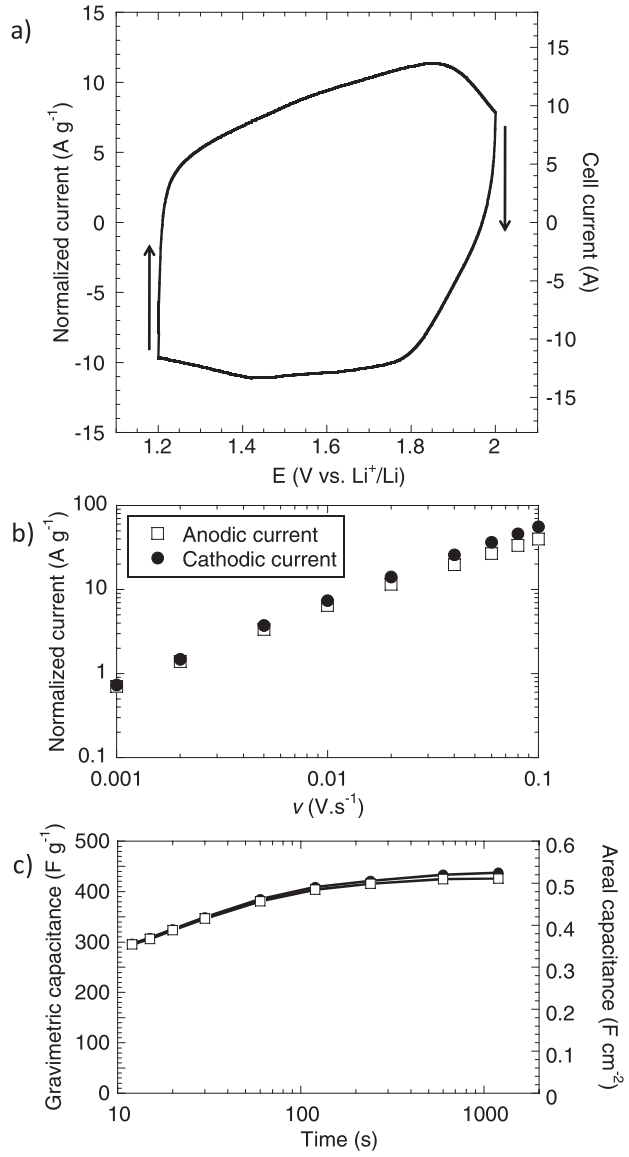

Figure 3. a) CV curve for a 40 μm-thick / 1.2 mg.cm^{-2} electrode at a sweep rate of 20 mV s^{-1}; b) cathodic and anodic currents as a function of sweep rate; c) gravimetrically normalized capacitance (F g^{-1}) and areal capacitance (F cm^{-2}) as a function of charge/discharge time.

In addition, composite films with a Nb_2O_5 mass loading up to 4 mg cm^{-2} were fabricated and cycled at 1 mV s^{-1} and 20 mV s^{-1} (Figure 4). Area-normalized capacitance values of 1.5 F cm^{-2} (425 F g^{-1}) and 0.98 F cm^{-2} (270 F g^{-1}) were measured for a 3.6 mg cm^{-2} film depending on rate. This shows that decent specific and areal capacitance values can be obtained for thick electrodes of Nb_2O_5 by using standard electrode formulation methods, Nonetheless, electrodes in the 4 mg cm^{-2} range exhibit a stronger sweep rate dependence compared to the 1.2 mg cm^{-2} electrodes shown in Figures 3b and 3c. The causes of the rate dependence are currently being studied as both ionic and electronic conductivities decrease upon increasing the sample loading. We tend to consider that the lower level of electronic conduction is more important here because Nb_2O_5 is a wide bandgap material and even upon lithium intercalation, the conductivity is on the order of 3 × 10^{-5} S cm^{-1}.[15] It is evident that improving the electrode formulation in terms of film composition (conducting agent and binder systems) as well as electrode fabrication and architecture will be necessary in order to achieve fast charge storage when the film thickness exceeds 40 μm.

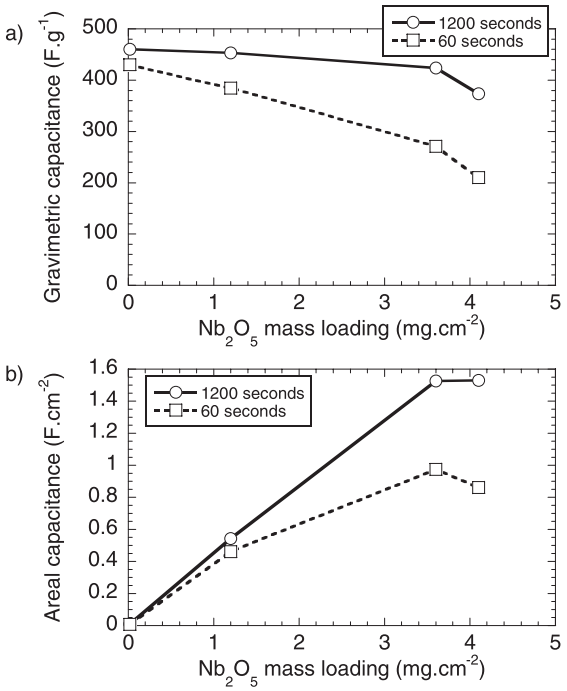

Figure 4. a) Gravimetric and b) areal capacitance as a function of the Nb_2O_5 mass loading. Values are determined from cyclic voltamograms at 1 mV s^{-1} and 20 mV s^{-1} corresponding to discharge times of 1200 and 60 seconds, respectively.

Nb_2O_5/activated carbon hybrid cell.— To highlight the benefits of using a high capacitance pseudocapacitive electrode, a hybrid cell comprised of a Nb_2O_5 negative electrode and an activated carbon positive electrode has been assembled and tested in 1M $LiClO_4$/PC electrolyte. The negative electrode mass loading was set to 1.5 mg cm^{-2}, and the positive one to 7 mg cm^{-2}. In this cell, the electrolyte is the only source for Li^+ and ClO_4^- ions. In a conventional system, ion consumption from the electrolyte must be taken into account to avoid ion depletion in the vicinity of the active particles.[34] In the study reported here, the salt concentration between both electrodes is considered to be in large excess, as the activated carbon electrode shows a maximum capacity of 30 mAh g^{-1} which corresponds to standard ion storage in a carbon/carbon cell. Hence, we consider here that the salt concentration in the electrolyte does not limit the kinetics of the electrochemical reaction. Figure 5a shows the charge/discharge curves of the hybrid cell in which the charge storage occurs between 0.8 V and 3 V, giving a higher average operating voltage than in symmetric carbon/carbon EDLCs. Meanwhile, the respective potentials of each electrode are recorded and shown in Figure 5b. A cell capacity as high as 70 F g^{-1} of total active material (negative and positive) was measured at a power of 300 W kg^{-1} of active material. Considering an active surface area of 1.1 cm^2, this capacitance translates to 0.5 F cm^{-2} in the device, approaching that of carbon/carbon EDLCs for high weight loading.[10,31,35,36]

The cell was subsequently tested under various charge–discharge currents. Figure 5c shows the Ragone plot (power vs. energy) of the Nb_2O_5/carbon hybrid cell compared to a symmetric carbon/carbon cell cycled between 0 V and 3 V in a LP30 electrolyte. In general, the energy density for the hybrid device was higher than that of the carbon/carbon cell, as 40 Wh kg^{-1} and 27 Wh kg^{-1} of total active material were measured at 300 W kg^{-1} (9 minutes) and 1500 W kg^{-1} (1 minute) charge/discharge powers, respectively. Long-term operation of the hybrid device showed very good cycling stability, with no observed energy loss after 1000 cycles at a 3000 W kg^{-1} (22 seconds) charge/discharge rate (Figure 5d). The excellent cycling stability is consistent with the small crystallographic changes in the Nb_2O_5 from

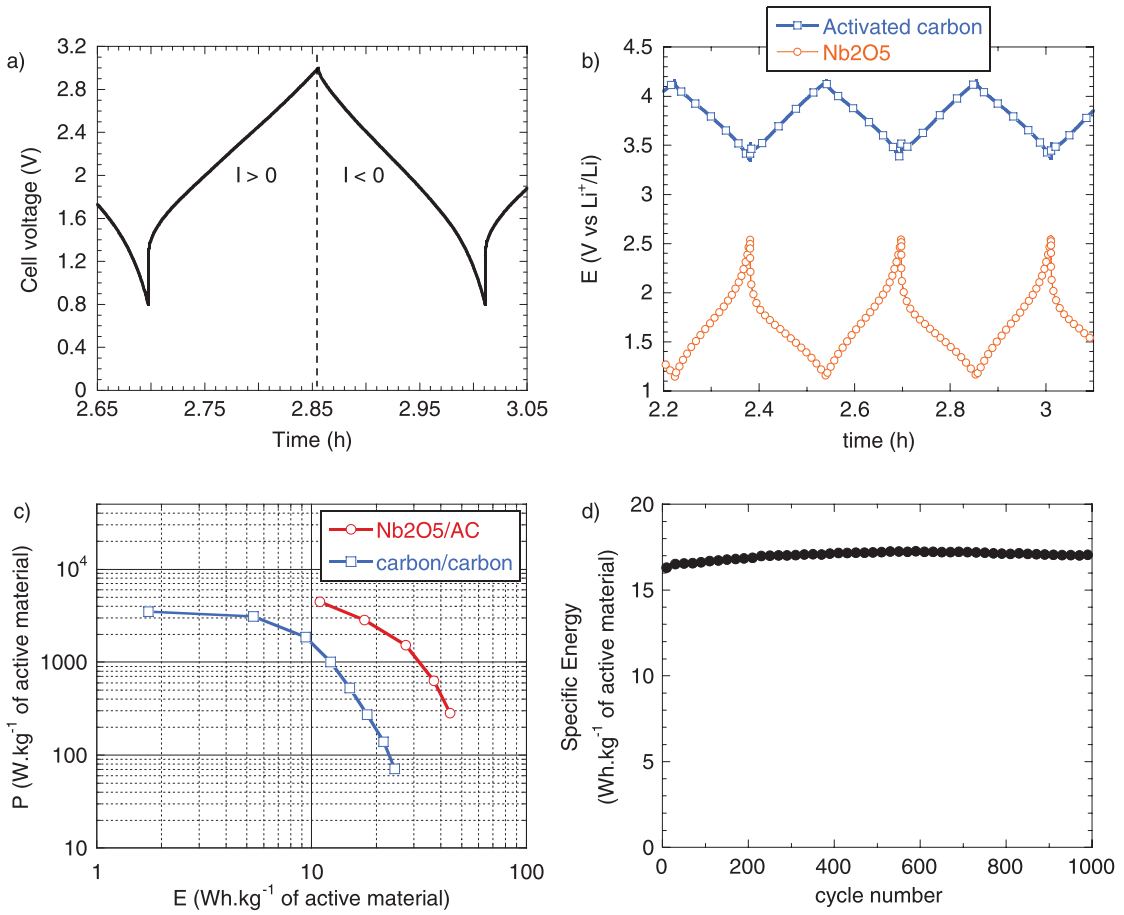

Figure 5. a) Charge/discharge curve of the Nb_2O_5/activated carbon hybrid cell cycled between 1 V and 3 V at 300 W kg^{-1} of total active material (positive and negative), b) corresponding charge/discharge curves of activated carbon positive electrode and Nb_2O_5 negative electrode, c) Ragone plot showing specific power vs. energy density of the hybrid cell compared with a carbon/carbon symmetric cell of comparable active material weight, d) cycling of the hybrid cell for 1000 cycles at 3000 W kg^{-1} shows no loss in energy.

Li^+ intercalation/deintercalation observed here and shown previously by Kumagai et al.[20]

Discussion.— The results obtained with the Nb_2O_5composite electrodes have significant implications for pseudocapacitor-based energy storage. First, the current work shows that the high-rate pseudocapacitive properties demonstrated with nanocrystalline Nb_2O_5 can be extended to practical electrode architectures. There are no diffusion limitations for charging times as short as one minute, and capacitive responses, e.g., rectangular voltammograms (Fig. 3a), are observed. Quantitatively, the composite Nb_2O_5 electrode retains a high level of specific capacitance, 380 F g^{-1}, at a sweep rate that corresponds to a one minute charge–discharge. This value is comparable to the 430 F g^{-1} obtained at the same sweep rate for the nanocrystalline Nb_2O_5 materials that rely on small dimensions (film thickness of < 100 nm) to achieve sufficient electronic conduction.[15] The in-situ XRD measurements made on the electrode confirm that charge storage with Nb_2O_5 is a bulk process and not confined to the surface. The change in *c*-axis lattice parameter upon Li^+ intercalation and de-intercalation is reversible, and for the maximum amount of Li^+ incorporation, $x = 1.8$, the *c*-axis parameter increase is on the order of only 3%. Although disordered, nanoscale RuO_2 also exhibits a pseudocapacitive voltammetric signature when cycled in non-aqueous Li^+-containing electrolyte.[37] The charge storage mechanism in this and other such cases is an adsorption-based process as compared to the Li^+ intercalation that occurs with Nb_2O_5.

The electrochemical behavior exhibited by the Nb_2O_5 electrodes provides a basis for distinguishing between different types of pseudocapacitive responses. Materials such as Nb_2O_5 that do not undergo any phase transformations during Li-ion intercalation can exhibit the characteristics of a pseudocapacitive process: *i*) a linear dependence of the open circuit potential with the state of charge; *ii*) an electrochemical process that is not limited by semi-infinite diffusion; and *iii*) a change in the oxidation state of the transition metal cation accompanied by high capacity values.[38,39] We consider such materials to be 'intrinsic pseudocapacitors.' In contrast, Li^+ intercalation materials that undergo at least one phase transition exhibit flat galvanostatic profiles where the potential is invariant with capacity over a wide region. In materials such as $LiCoO_2$,[40] $LiMn_2O_4$,[41] TiO_2,[42] and V_2O_5,[43,44] sloping galvanostatic profiles (and broadened CV peaks) in conjunction with improved rate capability can be observed, but only when the crystallite size is less than ~20 nm. The origin for these changes in the electrochemical behavior has been ascribed to the large number of surface sites in nanostructured materials, which leads to a range in energies for Li^+ positions near the surface. In such cases, the material's surface has been described as a "solid solution host to Li^+ intercalation."[45] These surface sites enable faster Li storage than sites located in the bulk, with the corresponding electrochemical behavior being that of a capacitor. We consider such responses to be representative of an 'extrinsic pseudocapacitor' (Figure 6a). The nanoscale crystallite size dependence is important if these extrinsically pseudocapacitive materials are to be used in practical electrochemical capacitor electrode architectures that are tens of microns thick. Another characteristic of extrinsic behavior is that extremely high gravimetrically-normalized specific capacitance values can be obtained when nanoscale films are used. As depicted in Figure 6a, a large concentration of cation

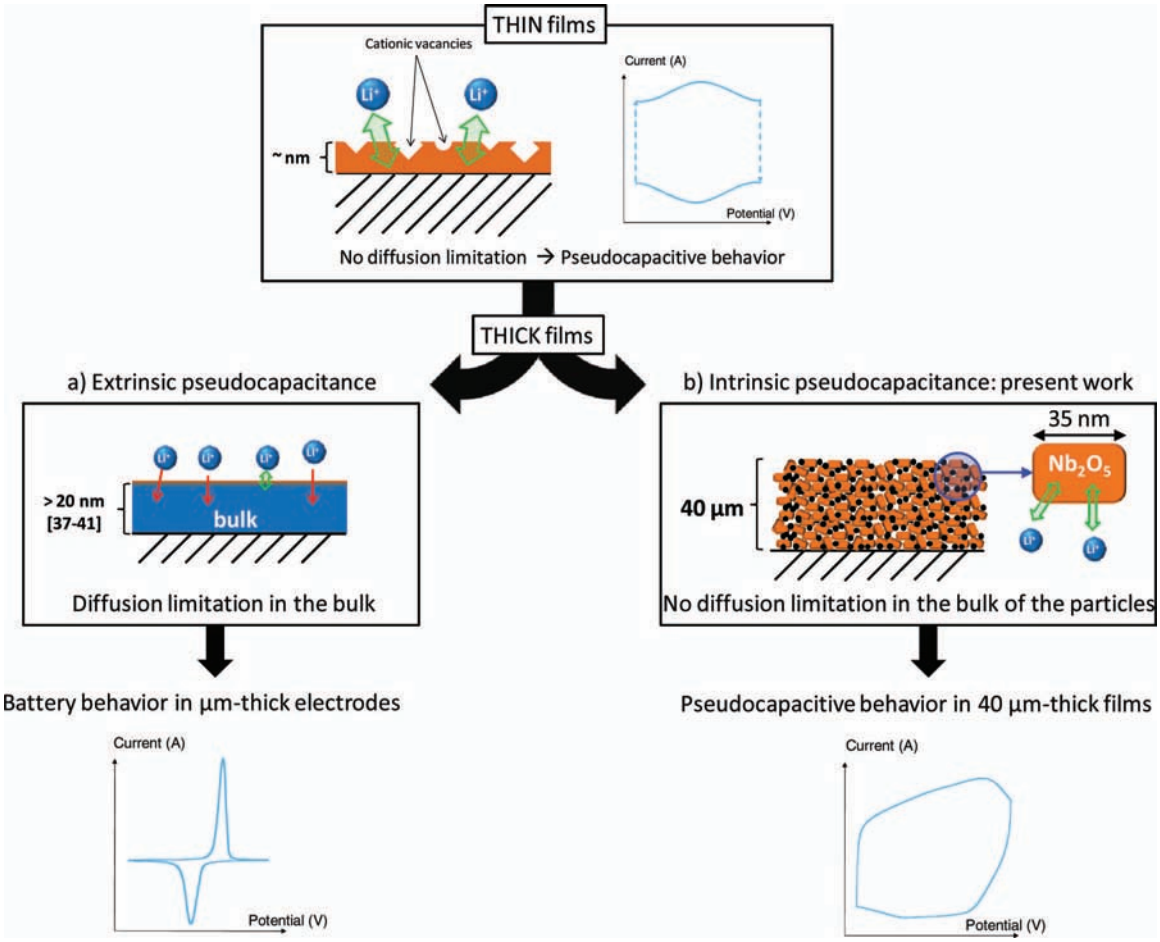

Figure 6. Schematic representations and corresponding electrochemical responses for 'extrinsic' and 'intrinsic' pseudocapacitors. a) Extrinsic pseudocapacitance where high specific capacitance values and pseudocapacitive behavior are observed only with thin films of the same material. The outer surface of the film dominates the response because of electrolyte access. A high concentration of defects at the surface (e.g., cation vacancies) will also contribute. This response is observed with most transition metal oxides; b) Intrinsic pseudocapacitance in Nb_2O_5. The pseudocapacitive behavior is preserved in thick films due to fast Li^+ transport within the bulk of the material.

vacancies may provide additional faradaic reaction sites for electrolyte cations.[46] This phenomenon has already been observed in V_2O_5 thin films,[43] where capacitance values have been measured that exceed theoretical values for two-electron insertion per V_2O_5 unit. Scaling extrinsic pseudocapacitors from nanoscale materials into microns-thick practical electrodes is a significant challenge. In order to retain the high specific capacitance of these redox-active materials upon Li^+ insertion, it is necessary to ensure that the nanoscale transition metal oxides are accessible to the electrolyte and effectively 'wired' to the electrode';[47] the latter arises from the addition of a conductive component. In contrast, the pseudocapacitance associated with Li^+ intercalation into Nb_2O_5 is preserved even when Nb_2O_5 is processed into practical electrode structures that are forty microns thick (Figure 3). There are no diffusion limitations in the electrode represented in Figure 6b. The intercalation pseudocapacitance observed with Nb_2O_5 is an intrinsic feature of this material, arising from fast Li^+ transport within the structure and reversible crystallographic changes.

In considering the fabrication of extrinsic or intrinsic pseudocapacitors into electrode architectures, it is important to emphasize the importance of the effect of film thickness on the rate properties and corresponding capacitance values of electroactive materials. Although some charge storage data are available for various film thicknesses, we are unaware of any comparisons that have been made among different materials. Accordingly, we compared Nb_2O_5 performance with the most widely studied pseudocapacitive transition metal oxides including MnO_2, RuO_2 and V_2O_5, and focused on the difference between thin and thick composite films. In making this comparison, it should be noted that we did not include several studies in which pseudocapacitive materials were incorporated into thick films by utilizing sophisticated architectures,[48,49] as this approach has had mixed success.[43] Moreover, electrochemical performance becomes dependent on such factors as the orientation of active material and current collector, as shown recently for birnessite MnO_x and spinel $LiMn_2O_4$.[50]

Table I lists gravimetric and areal capacitance values at different discharge rates for thin film materials (few µm-thick; $\leq$0.2 mg cm^{-2}). In this case, outstanding gravimetric capacitance values that surpass 1000 F g^{-1} and correspond to the full utilization of the material are measured at low discharge rates, and fairly high values can even be obtained in short times of less than one minute. However, the low mass loading of active material on the electrode leads to very low areal capacitance values, typically on the order of few mF cm^{-2}.

Examples of thick composite films ($>$10 µm-thick; $>$0.5 mg cm^{-2}) are listed in Table II. As expected, the areal capacitance of active films is increased at the expense of the gravimetric capacitance. For example, only 150 F g^{-1} is measured for MnO_2 100 µm-thick films in comparison to 1320 F g^{-1} for thin films.[32] This shows that in many reported cases, when the loading is on the order of 1 mg cm^{-2}, the resulting pseudocapacitor-based electrodes may require charge–discharge times well above one minute in order to retain the high specific capacitance of the transition metal oxide. Among the oxides listed here, hydrous RuO_2 exhibits the largest capacitance values in short times, but high cost renders it impractical for use in a viable

Table I. Gravimetric and areal capacitance for thin film/micro-device of pseudocapacitive transition metal oxides.

			Discharge time				
			> 2 min		≤ 1 min		
Oxide	Film thickness / oxide mass loading	Electrolyte	F g^{-1} of oxide	F cm^{-2}	F g^{-1} of oxide	F cm^{-2}	Ref
Nb_2O_5	20 μg cm^{-2}	1M $LiClO_4$/ PC	460	0.009	430	0.008	15
V_2O_5 on CNTs	10 nm	8M LiCl	1400	NC	1100	NC	33
V_2O_5	2 μm / 40 μg cm^{-2}	1M $LiClO_4$/ PC	300	0.012	200	0.008	51
MnO_2 on CNT	60 μg cm^{-2}	0.5M Na_2SO_4	410	0.025	310	0.019	52
MnO_2	< 5μm / 27 μg cm-2	0.1M Na_2SO_4	1320	0.036	NC	NC	32
$RuO_2.xH_2O$	200 μg cm^{-2}	0.1M H_2SO_4	1300	0.26	520	0.1	53

Table II. Gravimetric and areal capacitance for thick composite films of pseudocapacitive transition metal oxides.

			Discharge time				
			> 2 min		≤ 1 min		
Oxide	Film thickness / oxide mass loading	Electrolyte	F g^{-1} of oxide	F cm^{-2}	F g^{-1} of oxide	F cm^{-2}	Ref
Nb_2O_5	40μm / 1.2 mg cm^{-2}	1M $LiClO_4$/ PC	420	0.5	380	0.46	Presentwork
V_2O_5 on CNTs	30 nm	8M LiCl	410	Not communicated	300	Not communicated	33
V_2O_5Nanowires	∼100 μm / 3–5 mg cm^{-2}	1M $LiClO_4$/ PC	204	≤ 1	41	≤ 0.2	54
MnO_2 on CNT	1.3 mg cm^{-2}	0.5M Na_2SO_4	140	0.18	80	0.1	52
MnO_2	100μm / 2.0 mg cm^{-2}	0.1M Na_2SO_4	150	0.3	Not communicated	Not communicated	32
$RuO_2.xH_2O$	1.4 mg cm^{-2}	0.5M H_2SO_4	Not communicated	Not communicated	788	0.62	55

technology. With one exception, the other pseudocapacitor materials exhibit capacitances that do not scale with thicker electrode structures. The exception is Nb_2O_5. Even when Nb_2O_5 is processed using conventional slurry techniques into practical electrode structures that are tens of microns in thickness, the capacitance values associated with Li^+ intercalation into Nb_2O_5 remain high, even at high discharge/charge rates.

This comparison of gravimetric and areal capacitance values shows that even though Nb_2O_5 capacitor electrodes store charge by a bulk intercalation mechanism, the level of charge storage compares favorably with more traditional EDLC materials like activated carbon and exceeds that of most pseudocapacitive transition metal oxides. Although Nb_2O_5 cannot compete with carbon or MnO_2 in terms of cost, the potential advantage of Nb_2O_5 is that the development of pseudocapacitance involves the use of an organic electrolyte, thus leading to high operating voltages and the ability to design electrochemical energy storage systems with both high power and high energy.

Conclusions

The present work shows that the intercalation pseudocapacitance properties exhibited with nanocrystalline Nb_2O_5 can be extended to practical electrode architectures that are prepared using conventional slurry techniques. The high specific capacitance values and power capabilities of Nb_2O_5 electrodes do not arise from a surface effect but from fast Li^+ intercalation within the (00*l*) planes of the orthorhombic structure. Moreover, for charging times as fast as one minute, there are no diffusion limitations as measured in 40 μm-thick electrodes. The intercalation pseudocapacitance which leads to these extraordinary charge storage properties has been characterized as an intrinsic property of Nb_2O_5 which facilitates the design of electrodes containing pseudocapacitive materials. To further demonstrate the electrochemical properties of Nb_2O_5, we fabricated and characterized a hybrid cell using a Nb_2O_5 negative electrode. The device shows excellent performance with charging times shorter than one minute and down to few tens of seconds.

Acknowledgments

This work was supported by the Center for Molecularly Engineered Energy Materials, an Energy Frontier Research Center funded by the DOE Office of Basic Energy Sciences (DE-SC001342). J.C. was supported by Delegation Générale pour l'Armement (DGA). P.S. acknowledges the support from the European Research Council (ERC, Advanced grant, ERC-2011-AdG, Project 291543 – IONACES), the Chair of Excellence "Embedded multi-functional nanomaterials" from the EADS Foundation, as well as B. Duployer for precious support for the in-situ XRD experiments. J.W.L. acknowledges support from the U.S. Office of Naval Research.

References

1. P. Simon and Y. Gogotsi, *Nat. Mater.*, **7**, 845 (2008).
2. C. Largeot, C. Portet, J. Chmiola, P.-L. Taberna, Y. Gogotsi, and P. Simon, *J. Am. Chem. Soc*, **130**, 2730 (2008).
3. J. B. Goodenough and K.-S. Park., *J. Am. Chem. Soc.*, **135**, 1167 (2013).
4. B. E. Conway, *Electrochemical Supercapacitors*, Kluwer Academic/Plenum, New York, USA (1999).
5. Y. F. Yuan, X. H. Xia, J. B. Wu, J. L. Yang, Y. B. Chen, and S. Y. Guo, *Electrochim. Acta*, **56**, 2627 (2011).
6. O. Ghodbane, F. Ataherian, N.-L. Wu, and F. Favier, *J. Power Sources*, **206**, 454 (2012).
7. T. Brousse, M. Toupin, R. Dugas, L. Athouel, O. Crosnier, and D. Bélanger, *J. Electrochem. Soc.*, **153**, A2171 (2006).
8. A. Ghosh, E. J. Ra, M. Jin, H.-K. Jeong, T. H. Kim, C. Biswas, and Y. H. Lee, *Adv. Funct. Mater.*, **21**, 2541 (2011).
9. T. Brezesinski, J. Wang, S. H. Tolbert, and B. Dunn, *Nat. Mater.*, **9**, 146 (2010).
10. M. D. Stoller and R. S. Ruoff, *Energy Environ. Sci.*, **3**, 1294 (2010).
11. Y. Gogotsi and P. Simon, *Science*, **334**, 917 (2012).
12. B. Reichman and A. J. Bard, *J. Electrochem. Soc.*, **127**, 241 (1980).
13. R. Kodama, Y. Terada, I. Nakai, S. Komaba, and N. Kumagai, *J. Electrochem. Soc.*, **153**, A583 (2006).

14. N. Kumagai, Y. Koishikawa, S. Komada, and N. Koshiba, *J. Electrochem. Soc.*, **146**, 3203 (1999).
15. J. W. Kim, V. Augustyn, and B. Dunn, *Adv. Energy Mater.*, **2**, 141 (2012).
16. V. Augustyn, J. Come, M. A. Lowe, J. W. Kim, P.-L. Taberna, S. H. Tolbert, H. D. Abruña, P. Simon, and B. Dunn, *Nat. Mater.*, **12**, 518 (2013).
17. N. Q. Zhang, Z. M. Liu, T. Y. Yang, C. L. Liao, Z. J. Wang, and K. N. Sun, *Electrochem. Comm.*, **13**, 654 (2011).
18. M. Morcrette, Y. Chabre, G. Vaughan, G. Amatucci, J.-B. Leriche, S. Patoux, C. Masquelier, and J.-M. Tarascon, *Electrochim. Acta*, **47**, 3137 (2002).
19. C. Portet, P.-L. Taberna, P. Simon, and C. Laberty-Robert, *Electrochim. Acta*, **49**, 905 (2004).
20. R. Kodama, Y. Terada, I. Nakai, S. Komaba, and N. Kumagai, *J. Electrochem. Soc.*, **153**, A583 (2006).
21. K. Von Katsuo and S. Tamura, *Acta Crys. B*, **31**, 673 (1975).
22. A. A. Lubimtsev, P. R. C. Kent, B. G. Sumpterac, and P. Ganesh, *J. Mater. Chem. A*, **1**, 14951 (2013).
23. A. J. Bard and L. R. Faulkner, *Electrochemical Methods: fundamentals and applications*, 2nd ed., John Willey & Sons Inc., New-York (2001).
24. H. Lindström, S. Södergren, A. Solbrand, H. Rensmo, J. Hjelm, A. Hagfeldt, and S.-E. Lindquist, *J. Phys. Chem. B*, **101**, 7717 (1997).
25. J. Come, P.-L. Taberna, S. Hamelet, C. Masquelier, and P. Simon, *J. Electrochem. Soc.*, **158**, A1090 (2011).
26. A. Krause, P. Kossyrev, M. Oljaca, S. Passerini, M. Winter, and A. Balducci, *J. Power Sources*, **196**, 8836 (2011).
27. A. Balducci, U. Bardi, S. Caporali, M. Mastragostino, and F. Soavi, *Electrochem. Comm.*, **6**, 566 (2004).
28. T. E. Rufford, D. Hulicova-Jurcakova, E. Fiset, Z. Zhu, and G. Qing Lu, *Electrochem. Comm.*, **11**, 974 (2009).
29. P.-L. Taberna, C. Portet, and P. Simon, *Appl. Phys. A*, **82**, 639 (2006).
30. C. Largeot, P. L. Taberna, Y. Gogotsi, and P. Simon, *Electrochem. Sol. State Lett.*, **14**, A174 (2011).
31. J. Chmiola, C. Largeot, P.-L. Taberna, P. Simon, and Y. Gogotsi, *Angew. Chem. Int. Ed.*, **47**, 3392 (2008).
32. M. Toupin, T. Brousse, and D. Belanger, *Chem. Mater.*, **16**, 3184 (2004).
33. S. Boukhalfa, K. Evanoff, and G. Yushin, *Energy Environ. Sci.*, **5**, 6872 (2012).
34. J. P. Zheng, *J. Electrochem. Soc.*, **156**, A500 (2009).
35. J. Chmiola, G. Yushin, R. Dash, and Y. Gogotsi, *J Power Sources*, **158**, 765 (2006).
36. M. Olivares-Marín, J. A. Fernández, M. J. Lázaro, C. Fernández-González, A. Macías-García, V. Gómez-Serrano, F. Stoeckli, and T. A. Centeno, *Mat. Chem. Phys.*, **114**, 323 (2009).
37. J. C. Lytle, J. W. Long, K. A. Pettigrew, R. M. Stroud, and D. R. Rolison, *J. Mater. Chem.*, **17**, 1292 (2007).
38. B. E. Conway, *J. Electrochem. Soc.*, **138**, 1539 (1991).
39. B. E. Conway and W. G. Pell, *J. Solid State Electrochem.*, **7**, 637 (2003).
40. M. Okubo, E. Hosono, J. Kim, M. Enomoto, N. Kojima, T. Kudo, H. Zhou, and I. Honma, *J. Am. Chem. Soc.*, **129**, 7444 (2007).
41. T. J. Patey, R. Buchel, M. Nakayama, and P. Novak, *Phys. Chem. Chem. Phys.*, **11**, 3756 (2009).
42. J. Wang, J. Polleux, J. Lim, and B. Dunn, *J. Phys. Chem. C*, **111**, 14925 (2007).
43. M. Sathiya, A. S. Prakash, K. Ramesha, J.-M. Tarascon, and A. K. Shukla, *J. Am. Chem. Soc.*, **133**, 16291 (2011).
44. N. A. Chernova, M. Roppolo, A. C. Dillon, and M. S. Whittingham, *J. Mater. Chem.*, **19**, 2526 (2009).
45. A. G. Dylla, G. Henkelman, and K. J. Stevenson, *Acc. Chem. Res.*, **46**, 1104 (2013).
46. B. P. Hahn, J. W. Long, and D. R. Rolison, *Acc. Chem. Res.*, **45**, 1181 (2013).
47. S. Ardizzone, G. Fregonara, and S. Trasatti, *Electrochim. Acta*, **35**, 263 (1990).
48. D. R. Rolison, J. W. Long, J. C. Lytle, A. E. Fischer, C. P. Rhodes, T. M. McEvoy, M. E. Bourg, and A. M. Lubers, *Chem. Soc. Rev.*, **38**, 226 (2009).
49. J. W. Long, M. B. Sassin, C. N. Chervin, and D. R. Rolison, *Acc. Chem. Res.*, **45**, 1062 (2013).
50. M. B. Sassin, S. G. Greenbaum, P. E. Stallworth, A. N. Mansour, B. P. Hahn, K. A. Pettigrew, D. R. Rolison, and J. W. Long, *J. Mater. Chem. A*, **1**, 2431 (2013).
51. I.-H. Kim, J.-H. Kim, B.-W. Cho, Y.-H. Lee, and K.-B. Kim, *J. Electrochem. Soc.*, **153**, A989 (2006).
52. L. Hu, W. Chen, X. Xie, N. Liu, Y. Yang, H. Wu, Y. Yao, M. Pasta, H. N. Alshareef, and Y. Cui, *ACS Nano*, **5**, 8904 (2011).
53. C.-C. Hu, K.-H. Chang, M.-C. Lin, and Y.-T. Wu, *Nano Letters*, **6**, 2690 (2006).
54. Z. Chen, V. Augustyn, J. Wen, Y. Zhang, M. Shen, B. Dunn, and Y. Lu, *Adv. Mater.*, **23**, 791 (2011).
55. B.-O. Park, C. D. Lokhande, H.-S. Park, K.-D. Jung, and O.-S. Joo, *J. Power Sources*, **134**, 148 (2004).